

Angle-resolved photoemission spectroscopy of Na-doped $\text{Ca}_2\text{CuO}_2\text{Cl}_2$ single crystals: Fingerprints of a magnetic insulator in a heavily underdoped superconductor

Y. Kohsaka,¹ T. Sasagawa,^{1,2} F. Ronning,³ T. Yoshida,³ C. Kim,³ T. Hanaguri,^{1,2} M. Azuma,⁴ M. Takano,⁴ Z.-X. Shen,³ and H. Takagi¹

¹*Department of Advanced Materials Science, University of Tokyo, 7-3-1 Hongo, Bunkyo-ku, Tokyo 113-0033, Japan*

²*SORST, Japan Science and Technology Corporation, Kawaguchi, Saitama 332-0012, Japan*

³*Geballe Laboratory for Advanced Materials, Department of Physics, Applied Physics, and Stanford Synchrotron Radiation Laboratory, Stanford University, Stanford, California 94305, USA*

⁴*Institute for Chemical Research, Kyoto University, Uji, Kyoto-fu 611-0011, Japan*

(October 28, 2018)

Electronic evolution from an antiferromagnet to a high- T_c superconductor is revealed by angle-resolved photoemission experiments on tetragonal $\text{Ca}_{1.9}\text{Na}_{0.1}\text{CuO}_2\text{Cl}_2$ single crystals, which were successfully grown for the first time under high pressures. In this underdoped superconductor, we found clear fingerprints of the parent insulator: a shadow band and a large pseudo-gap. These observations are most likely described by a “chemical potential shift”, which contrasts clearly with the prevailing wisdom of the “pinned chemical potential” learned from the prototype $\text{La}_{2-x}\text{Sr}_x\text{CuO}_4$, demonstrating that the route to a high- T_c superconductor is not unique.

PACS numbers: 74.25.Jb, 71.18.+y, 74.72.Jt, 79.60.-i

Elucidating the mechanism of high- T_c superconductivity (HTS) has been one of the most attractive challenges in condensed matter physics today. A key ingredient for HTS is the two dimensional CuO_2 plane, which, upon carrier doping, switches from an antiferromagnetic insulator to HTS. An important step towards solving the HTS puzzle is to understand the electronic evolution across the insulator to metal transition. Angle-resolved photoemission spectroscopy (ARPES) is one of the most powerful tools to do this, as it can measure the momentum dependent electron excitation spectrum directly. So far, because of their superior surface quality associated with an easy cleavage plane, most ARPES studies have been conducted on $\text{Bi}_2\text{Sr}_2\text{Ca}_{n-1}\text{Cu}_n\text{O}_y$ ($n = 1, 2$). In Bi cuprates, however, it is not easy to access the composition in the vicinity of the insulator-metal transition. This has been preventing us from attacking the fundamental issue of electronic evolution from parent insulator to HTS. At present, most information regarding this issue stems from $\text{La}_{2-x}\text{Sr}_x\text{CuO}_4$, where two electronic components and pinning of the chemical potential have been observed [1,2]. It is of great interest to study whether the results from $\text{La}_{2-x}\text{Sr}_x\text{CuO}_4$ are universal.

Alkaline-earth copper oxychlorides, $\text{A}_2\text{CuO}_2\text{Cl}_2$ ($\text{A} = \text{Ca}, \text{Sr}$), have been known as an ideal parent insulator. They have a simple tetragonal K_2NiF_4 -type structure with *undistorted* and *single* CuO_2 planes. Their single crystals can be cleaved very easily, and, indeed, the best ARPES data on insulators have been obtained on these systems [3,4,5,6]; e.g., a *d*-wave-like dispersion of the Mott gap was disclosed [6]. Due to the success in the parent insulator, single crystals of oxychlorides doped with mobile carriers have been envisaged to explore the evolution of the Fermi surface from the *d*-wave-like Mott gap [7]. Hole-doped $\text{Ca}_2\text{CuO}_2\text{Cl}_2$ can be realized by substituting Na^+ for Ca^{2+} . $\text{Ca}_{2-x}\text{Na}_x\text{CuO}_2\text{Cl}_2$ shows superconductivity ($T_c^{\text{max}} = 28$ K at $x \sim 0.2$) but forms

only under high pressures of several GPa [8,9]. Previous attempts to grow single crystals of $\text{Ca}_{2-x}\text{Na}_x\text{CuO}_2\text{Cl}_2$ have been unsuccessful, mainly because of the difficulty in the crystal growth under high pressures. Recently, we have succeeded in growing $\text{Ca}_{2-x}\text{Na}_x\text{CuO}_2\text{Cl}_2$ single crystals for the first time using a specially designed high pressure furnace [10].

In this Letter, we report the first ARPES data on superconducting, $\text{Ca}_{1.9}\text{Na}_{0.1}\text{CuO}_2\text{Cl}_2$ single crystals, which demonstrate that the band dispersion of the doped oxychloride is a consequence of the valence band of the parent insulator shifting to the chemical potential. The resulting fingerprints of the parent insulator manifest itself in the way of a shadow band and a large pseudo-gap. These results are remarkably different from the prevailing picture proposed for the prototypical HTS material, $\text{La}_{2-x}\text{Sr}_x\text{CuO}_4$, where the chemical potential remains fixed while new states are created around it by doping. This indicates that the electronic evolution across the insulator to metal transition is not unique among HTS's.

The $\text{Ca}_{2-x}\text{Na}_x\text{CuO}_2\text{Cl}_2$ crystals used in this study were prepared by a flux growth [10]. A powder mixture of $\text{Ca}_2\text{CuO}_2\text{Cl}_2 + 0.2\text{NaCl} + 0.2\text{NaClO}_4$ was heated and slowly cooled under a pressure of 4 GPa. Thin plate like crystals, shown in the inset of Fig. 1, were obtained from the solidified melt. They were easily cleaved like mica, which was the key to the success of the present ARPES study. Their Na content, x , was estimated to be 0.1 from x-ray diffraction and electron-probe-microanalysis measurements [10]. Superconductivity in these crystals was confirmed by both resistivity (Fig. 1) and magnetization measurements. The transition temperature of $T_c = 13$ K is in good agreement with $x \sim 0.1$ powder results [9]. Since the onset of superconductivity in $\text{Ca}_{2-x}\text{Na}_x\text{CuO}_2\text{Cl}_2$ is reported to occur at $x \sim 0.07$ [9,10], the samples with $x = 0.1$ are located just beyond the insulator-metal transition, corresponding to

a heavily underdoped superconductor.

The ARPES measurements were performed at beamline 5-4 of the Stanford Synchrotron Radiation Laboratory. The data were collected using a SES-200 hemispherical analyzer with a monochromated synchrotron beam (16.5 \sim 25.5 eV photons) or a He lamp (21.2 eV photons). The angular and energy resolution was 0.25 $^\circ$ and \leq 16 meV, respectively. At the end of the ARPES measurements, low-energy electron diffraction (LEED) was measured at 20 K. The four-fold symmetry of the LEED pattern without any super-lattice diffraction (the inset of Fig. 1, bottom right) confirms that the crystal structure is tetragonal and that there is no surface reconstruction also in the Na-doped $\text{Ca}_2\text{CuO}_2\text{Cl}_2$ compound.

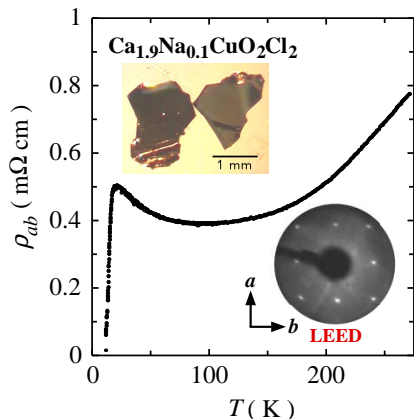


FIG. 1. Temperature dependence of the ab -plane resistivity for the $\text{Ca}_{1.9}\text{Na}_{0.1}\text{CuO}_2\text{Cl}_2$ single crystal. Insets: Photograph of $\text{Ca}_{1.9}\text{Na}_{0.1}\text{CuO}_2\text{Cl}_2$ crystals grown by the flux method under 4 GPa (top left), and the low-energy electron diffraction pattern measured at 20 K (bottom right).

We begin with an examination of the raw ARPES data at 20 K along the high symmetry directions as shown in Figure 2. The spectra in Fig. 2(a) show that a peak is moving up towards the Fermi level E_F on going from $(0,0)$ to (π,π) . Slightly before $(\pi/2,\pi/2)$, the peak reaches E_F and a sharp cutoff is clearly seen in the spectra. This is evidence for a Fermi level crossing, indicating that the Na-doping successfully changes the oxychloride into a metal. However, taking a further look at Fig. 2(a), we notice something unusual is happening around $(\pi/2,\pi/2)$. After the Fermi level crossing, a broad feature remains and is pulling away from E_F , though losing weight rapidly. The presence of a band dispersing back near $(\pi/2,\pi/2)$, a shadow band, is strongly reminiscent of that in the parent insulator, where a band folding occurs at $(\pi/2,\pi/2)$ because of the unit cell doubling due to an antiferromagnetic ordering. Because no change in the symmetry of the crystal structure was confirmed by the LEED measurements [inset of Fig. 1], the most likely source of the band folding is antiferromagnetic correlations still remaining in the carrier-doped metallic samples. Due to the presence of

a structural modulation, the origin of the shadow band previously reported in $\text{Bi}_2\text{Sr}_2\text{CaCuO}_y$ [11] has been controversial. In this context, the present observation unambiguously shows that, even without any lattice distortion, the shadow band can be present. In addition to the magnetic shadow band, we notice that the fine structure of the spectra near $(\pi/2,\pi/2)$ is more complicated than the simple Fermi cutoff. As indicated by tick-marks in Fig. 2(a), the spectra very close to the Fermi crossing consists of not a single component but two components: a sharp quasiparticle peak and a broad hump, which are quite similar to the “peak-dip-hump” structure observed in other HTS materials [12,13,14,15,16]. We will discuss this peak-dip-hump like structure in more detail later.

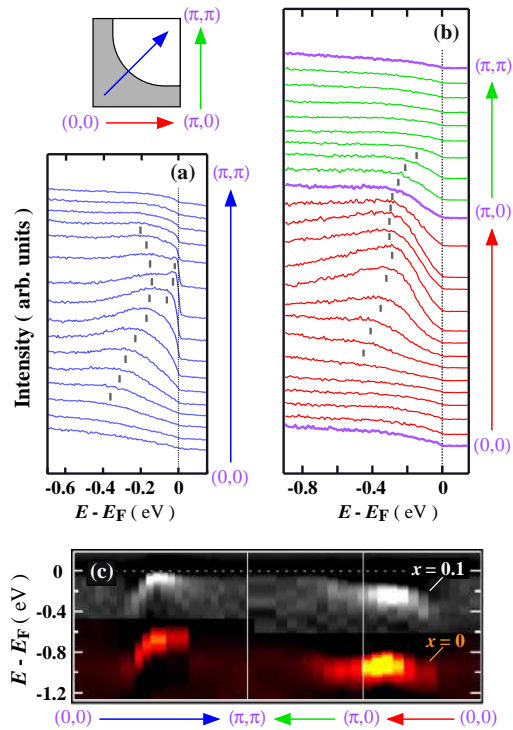


FIG. 2. The ARPES spectra in the $\text{Ca}_{1.9}\text{Na}_{0.1}\text{CuO}_2\text{Cl}_2$ single crystal; (a) along $(0,0)$ to (π,π) , (b) along $(0,0)$ to $(\pi,0)$ to (π,π) . Shown in the top-left is the Brillouin zone with a schematic hole-like Fermi surface. (a) An intensity plot of the second derivative of the spectra for $\text{Ca}_{2-x}\text{Na}_x\text{CuO}_2\text{Cl}_2$. The data for the parent insulator ($x = 0$) [6] are reproduced for comparison.

We observe unusual features also around $(\pi,0)$: almost complete loss of spectral weight at E_F over an extremely large energy scale of a tenth of an eV. The ARPES spectra from $(0,0)$ to $(\pi,0)$ to (π,π) are displayed in Fig. 2(b). A broad peak, which is very weakly dependent on the momentum near $(\pi,0)$, is apparent. In the case of the hole-like Fermi surface expected from band theory, schematically shown in Fig. 2, the dispersion should reach E_F on going from $(\pi,0)$ to (π,π) . In contrast to the unambiguous Fermi level crossing in the diagonal direction

[Fig. 2(a)], such behavior is not observed in Fig. 2(b). Instead, the broad feature simply appears to lose weight and vanishes completely on its approach to E_F . The lack of a well-defined Fermi surface near $(\pi,0)$ has been ascribed to a pseudo-gap. Remarkably, in comparison with other HTS's, the energy scale of the pseudo-gap in $\text{Ca}_{1.9}\text{Na}_{0.1}\text{CuO}_2\text{Cl}_2$ is extremely large and distinct as a HTS material. The leading edge midpoint of the spectra at $(\pi,0)$, which has often been used as a measure of the pseudo-gap, gives a value of 130 meV, which should be compared with 30 meV for $\text{Bi}_2\text{Sr}_2\text{Ca}_{1-x}\text{Dy}_x\text{Cu}_2\text{O}_y$ at a similar doping level ($x = 0.1$) [17]. The value of the leading edge midpoint along $(\pi,0)$ to (π,π) reaches its minimum of 65 meV around $(\pi,\pi/3)$. Note that the observed pseudo-gap magnitude is almost identical with the energy scale of the d -wave-like dispersion in the parent insulator [6].

To better visualize the band dispersion, the intensity of the second derivative of the spectra in Figs. 2(a) and 2(b) is mapped on the momentum vs. energy plane in Fig. 2(c). Around E_F , we see more clearly the band dispersing back near $(\pi/2,\pi/2)$ (the shadow band) as well as the missing weight near $(\pi,0)$ (the extremely large pseudo-gap). We argue that these anomalous features seen in the $\text{Ca}_{1.9}\text{Na}_{0.1}\text{CuO}_2\text{Cl}_2$ crystal originate from the parent insulator. To make our point, it may be instructive to compare the $\text{Ca}_{1.9}\text{Na}_{0.1}\text{CuO}_2\text{Cl}_2$ with the parent insulator. In Fig. 2(c), we also reproduce the band dispersion of the parent insulator. Immediately we notice that these two sets of dispersion are nearly identical and overlap with each other if we shift the dispersion of the parent insulator by ~ 700 meV. This indicates that, upon doping, the chemical potential simply drops to the top of the valence band, resulting in the shadow band near $(\pi/2,\pi/2)$ and the large pseudo-gap around $(\pi,0)$. This provides very clear evidence that the “large” pseudo-gap in the heavily underdoped region is intimately linked with the d -wave-like dispersion of the Mott gap.

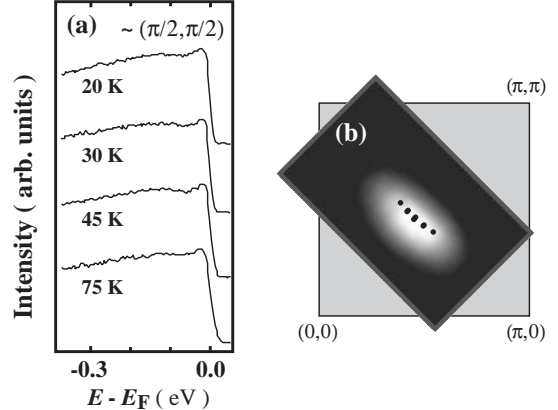


FIG. 3. (a) Temperature dependence of ARPES spectra at $\sim(\pi/2, \pi/2)$ in the $\text{Ca}_{1.9}\text{Na}_{0.1}\text{CuO}_2\text{Cl}_2$ single crystal. (b) Image plot of the integrated ARPES spectral weight over a 100 meV window below E_F . Superimposed dots are k -space locations of the sharp peaks observed in the ARPES spectra.

In the rigid band shift scenario, the dispersion closest to E_F in the parent insulator [i.e., near $(\pi/2,\pi/2)$] touches E_F to form the Fermi surface by carrier-doping, switching its state into a metal (superconductor). As seen in Fig 2(a), the Fermi crossing is indeed observed near $(\pi/2,\pi/2)$ in $\text{Ca}_{1.9}\text{Na}_{0.1}\text{CuO}_2\text{Cl}_2$, with additional low-energy structure in the spectra. It is found that the peak-dip-hump like structure in $\text{Ca}_{1.9}\text{Na}_{0.1}\text{CuO}_2\text{Cl}_2$ is robust at temperature far above $T_c = 13$ K [Fig. 3(a)]. The peak-dip-hump like structure observed in $\text{Ca}_{1.9}\text{Na}_{0.1}\text{CuO}_2\text{Cl}_2$ differs from that in $\text{Bi}_2\text{Sr}_2\text{CaCu}_2\text{O}_y$ in two ways [12]. Here it is observed in the nodal direction and above T_c , while in $\text{Bi}_2\text{Sr}_2\text{CaCu}_2\text{O}_y$ it is observed at $(\pi,0)$ and below T_c . There have been several proposals for the origin of the peak-dip-hump structure in the spectral lineshape of $\text{Bi}_2\text{Sr}_2\text{CaCu}_2\text{O}_y$, many resulting from a coupling of the quasiparticles with some collective modes [14,15,16]. The present results are quite different from the drastic change in the $(\pi,0)$ spectra across T_c in $\text{Bi}_2\text{Sr}_2\text{CaCu}_2\text{O}_y$ [12,13], and further experiments such as the doping dependence study will be helpful in elucidating the origin of this feature.

Now, let us examine the overall distribution of the low-energy excitations in momentum space. To distinguish different energy scales of contributions, we adopted two methods. One is the gray scale intensity plot obtained by integrating the spectral-weight over a 100 meV window below E_F as shown in Figure 3(b). The majority of the intensity lies about $(\pi/2,\pi/2)$, mainly because the large pseudo-gap removes most of the low-energy spectral weight around $(\pi,0)$. This intensity plot with a large energy-integration window gives a rather broad structure around $(\pi/2,\pi/2)$, which extends not only towards $(0,0)$ but also towards (π,π) . This reflects the presence of the shadow band from $(\pi/2,\pi/2)$ to (π,π) . The observed dis-

tribution of spectral weight is consistent with the most naive picture of a rigid band shift. In this scenario, we would expect the insulating bands with a maximum at $(\pi/2, \pi/2)$ to be simply cut by the Fermi function, creating a small Fermi surface pocket around $(\pi/2, \pi/2)$. If we extract the contribution only from the vicinity of E_F , however, the map looks drastically different. We roughly estimated this low energy excitations by plotting the k -points where the sharp peak is observed. As shown by the dots in Fig. 3(b), the sharp peaks form a Fermi surface in the form of an “arc” rather than a “pocket”.

We briefly consider here a few theories which appear particularly relevant to this system. In a theory where umklapp scattering is believed to create gaps about $(\pi, 0)$ in both the spin and charge channels, Fermi arcs have been predicted which appear consistent with the present data in Fig. 3(b) [18]. However, the shadow band demonstrated in Fig. 2 seems to escape this formalism. Alternatively, the RVB flux phase [19], or the more general arguments made by Chakravarty *et al.* [20], naturally contains shadow bands. In this case the Fermi surface is predicted to appear as four hole pockets centered about $(\pm\pi/2, \pm\pi/2)$. However, only the Fermi surface segment associated with the main band contains additional electronic structure (coherent-like peak), while that with the shadow band does not. This may provide a natural starting point for the pocket to evolve into the large Fermi surface without shadow Fermi surface.

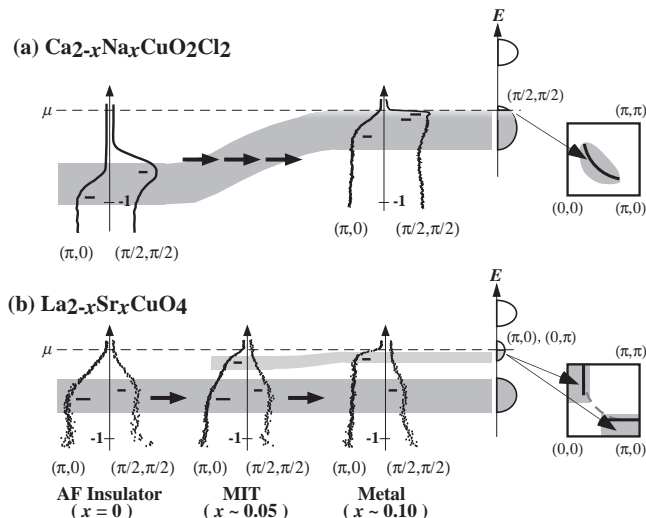


FIG. 4. Two distinct routes of the electronic evolution in the CuO_2 plane from a magnetic insulator to an underdoped superconductor: (a) $\text{Ca}_{2-x}\text{Na}_x\text{CuO}_2\text{Cl}_2$ and (b) $\text{La}_{2-x}\text{Sr}_x\text{CuO}_4$ [2]. The changes in the ARPES spectra upon carrier doping at $(\pi, 0)$ and $(\pi/2, \pi/2)$ are shown, illustrating the contrast between the chemical potential shift for $\text{Ca}_{2-x}\text{Na}_x\text{CuO}_2\text{Cl}_2$ and the fixed chemical potential for $\text{La}_{2-x}\text{Sr}_x\text{CuO}_4$. The resulting distribution of low energy ARPES spectral weight (an energy window of 100 meV) over k -space is schematically shown for metallic compounds.

Experimentally, the picture that emerges from the

present data differs significantly from the electronic evolution recently reported for $\text{La}_{2-x}\text{Sr}_x\text{CuO}_4$ [1,2,21]. Figure 4 demonstrates the comparison of the doping dependence of ARPES spectra between $\text{Ca}_{2-x}\text{Na}_x\text{CuO}_2\text{Cl}_2$ and $\text{La}_{2-x}\text{Sr}_x\text{CuO}_4$ [2] at $(\pi/2, \pi/2)$ and $(\pi, 0)$. In the undoped compounds, both La_2CuO_4 and $\text{Ca}_2\text{CuO}_2\text{Cl}_2$, the broad peaks far below E_F represent the insulating gap with the d -wave-like dispersion [6]. In the case of $\text{La}_{2-x}\text{Sr}_x\text{CuO}_4$ [Fig. 4(b)], the features of the insulator remain at the same energy upon doping while new states are created inside the gap as seen in the $(\pi, 0)$ spectrum [1,2]. This duality indicates that the chemical potential is *fixed* upon doping. As summarized in Fig. 4(a), the situation in the doped oxychloride is strikingly different. The evolution of the electronic states in this system can be understood roughly by a shift of the chemical potential to the top of the valence band. Intimately linked with the difference in the electronic evolution, the distribution of the spectral-weight in momentum space contrasts substantially between the two systems. As illustrated in Fig. 4, the predominance of the low energy spectral weight in metallic $\text{La}_{1.9}\text{Sr}_{0.1}\text{CuO}_4$ occurs near $(\pi, 0)$ and $(0, \pi)$ [21], while it occurs near $(\pi/2, \pi/2)$ in the metallic $\text{Ca}_{1.9}\text{Na}_{0.1}\text{CuO}_2\text{Cl}_2$.

The duality of $\text{La}_{2-x}\text{Sr}_x\text{CuO}_4$, together with the 1D nature of the $(\pi, 0)$ Fermi surface and the lack of the chemical potential shift, has been linked with stripe formation [1,2,21]; a phase separation into 1D charge and spin stripes. The rigid band shift of the oxychlorides suggests that antiferromagnetic fluctuations, originating from the parent insulator, instead dominate the metallic region for oxychlorides. Why is the oxychloride system so distinct from $\text{La}_{2-x}\text{Sr}_x\text{CuO}_4$? Structurally, the main difference between the two lies in the apical site (Cl vs. O) and the distortion of the CuO_2 planes (undistorted vs. distorted). These slight structural differences might help stabilize various different phases, resulting in enhanced antiferromagnetic correlations in the oxychlorides. In any event, the doped oxychloride system provides a new paradigm in the electronic evolution not previously observed in the cuprates. Surprisingly, however, the appearance of HTS upon doping does not crucially depend on which path leads the parent insulator to a metal.

We would like to thank A. Ino, A. Fujimori, T. Tohyama, S. Maekawa, N. Nagaosa, S. Uchida, and K. Kitazawa for fruitful discussions. This work was partly supported by a Grant-in-Aid for Scientific Research from the MEXT, Japan. ARPES experiments were carried out at SSRL, a national user facility operated by Stanford University on behalf of the U.S. DOE.

- [1] A. Ino *et al.*, Phys. Rev. Lett. **79**, 2101 (1997).
 [2] A. Ino *et al.*, Phys. Rev. B **62**, 4137 (2000).

- [3] B. O. Wells *et al.*, Phys. Rev. Lett. **74**, 964 (1995).
- [4] S. LaRosa *et al.*, Phys. Rev. B **56**, R525 (1997).
- [5] C. Kim *et al.*, Phys. Rev. Lett. **80**, 4245 (1998).
- [6] F. Ronning *et al.*, Science **282**, 2067 (1998).
- [7] H. Takagi, Physica (Amsterdam) **341C-348C**, 3 (2000).
- [8] Z. Hiroi, N. Kobayashi, and M. Takano, Nature (London) **371**, 139 (1994).
- [9] Z. Hiroi, N. Kobayashi, and M. Takano, Physica (Amsterdam) **266C**, 191 (1996).
- [10] Y. Kohsaka *et al.* J. Am. Chem. Soc., in press.
- [11] P. Aebi *et al.* Phys. Rev. Lett. **72**, 2757 (1994).
- [12] D. S. Dessau *et al.*, Phys. Rev. Lett. **66**, 2160 (1991).
- [13] D. L. Feng *et al.*, Science **289**, 277 (2000).
- [14] H. Ding *et al.*, Phys. Rev. Lett. **76**, 1533 (1996).
- [15] J. C. Campuzano *et al.*, Phys. Rev. Lett. **83**, 3709 (1999).
- [16] A. Lanzara *et al.*, Nature (London) **412**, 510 (2001).
- [17] D. S. Marshall *et al.*, Phys. Rev. Lett. **76**, 4841 (1996).
- [18] N. Furukawa, T. M. Rice, and M. Salmhofer, Phys. Rev. Lett. **81**, 3195 (1998).
- [19] X. -G. Wen and P. A. Lee, Phys. Rev. Lett. **76**, 503 (1996).
- [20] S. Chakravarty *et al.*, Phys. Rev. B **63**, 094503 (2001).
- [21] X. J. Zhou *et al.*, Science **286**, 268 (1999).